Science of the Total Environment 722 (2020) 137749

Contents lists available at ScienceDirect

Science of the Total Environment

journal homepage: www.elsevier.com/locate/scitotenv

Controls on the persistence of aqueous-phase groundwater contaminants in the presence of reactive back-diffusion

Landon J.S. Halloran *, Daniel Hunkeler

Centre d'Hydrogéologie et de Géothermie (CHYN), Université de Neuchâtel, Switzerland

HIGHLIGHTS

- Competing controls on plume persistence evaluated via parameter space investigation.
- Concentration maxima and attenuation times calculated for different scenarios.
- Effects of advection, diffusion, sorption, degradation and layer thickness tested.
- Plume persistence results show relative influences of different processes.
- Lower limit on plume extent is established via new combined parameter.

GRAPHICAL ABSTRACT

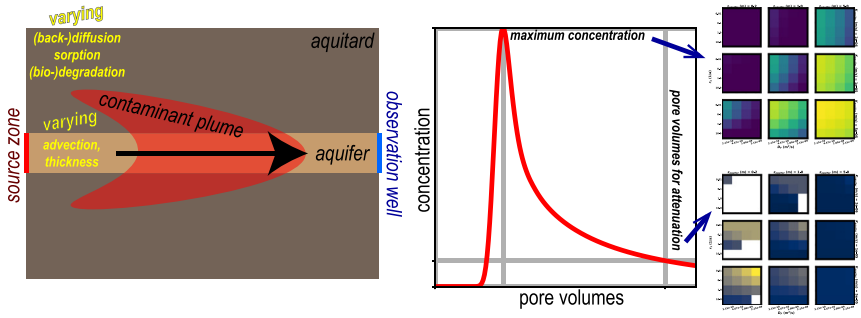

ARTICLE INFO

Article history:
Received 17 January 2020
Received in revised form 3 March 2020
Accepted 3 March 2020
Available online 9 March 2020

Editor: Damia Barcelo

Keywords:
Plume persistence
Back-diffusion
Sorption
Sensitivity analysis
Groundwater contaminants
Reactive transport

ABSTRACT

The persistence of groundwater contaminants is influenced by several interacting processes. Physical, physico-chemical, and (bio-)chemical processes all influence the transport of contaminants in the subsurface. However, for a given hydrogeological system, it is generally unclear to which degree each of these phenomena acts as a control on plume behaviour. Here, we present a comprehensive investigation of these processes and their influences on plume behaviour and persistence in layered sedimentary systems. We investigate different scenarios that represent fundamental configurations of common contaminant situations. A confined aquifer over- and underlain by aquitard layers is investigated in a source-removal scenario and a constant-source equilibrium scenario. Additionally, an aquitard overlain and underlain by high permeability units is investigated in a source-removal scenario. In these investigations, we vary layer thickness, as well as parameters governing advection, (back-) diffusion, sorption, and degradation. Extensive analysis of these results enables quantification of the influence of these parameters on maximum down-gradient concentration, plume persistence duration, and plume spatial extent. Finally, parameter space dimensionality reduction is used to establish trends and regimes in which certain processes dominate as controls. A lower limit to plume extent as a function of a novel constructed parameter is also determined. These results provide valuable quantitative information for the assessment of the fate of groundwater contaminants and are applicable to a wide range of aqueous-phase solutes.

1. Introduction

Aqueous-phase contaminant plumes are problematic and common in sedimentary systems (Eberhardt and Grathwohl, 2002; Adamson

* Corresponding author at: CHYN, Université de Neuchâtel, rue Émile-Argand 11, 2000 Neuchâtel, Switzerland.
E-mail address: landon.halloran@unine.ch (L.J.S. Halloran).

https://doi.org/10.1016/j.scitotenv.2020.137749
0048-9697/

et al., 2014; Kaplan et al., 2014; Zakari et al., 2016). Management of these sites is often challenging due to the various interacting processes that control plume behaviour. These controlling mechanisms can be physical, physio-chemical, chemical/bio-chemical, and spatial (Rao et al., 2002; Majone et al., 2015; Wanner et al., 2018b). Back-diffusion is the phenomenon wherein a solute, which may be groundwater contaminant, diffuses from a low-permeability unit (aquitard) to a high-permeability unit (aquifer) (Parker et al., 2008). This occurs when the concentration gradient is reversed after a contaminant source has diffused into the aquitard from the aquifer. This gradient reversal can occur due to propagation of contaminant plume, as well as due to attenuation or removal of the contaminant source. Back-diffusion complicates remediation efforts because it causes contaminant concentrations in the aquifer to remain higher than they would be in an otherwise isolated aquifer (Parker et al., 2008; Seyedabbasi et al., 2012; Yang et al., 2015).

Back-diffusion has been routinely observed in unconsolidated sedimentary systems with alternating low permeability (often clay-rich) and high permeability sandy layers (e.g., Parker et al., 2008; Yang et al., 2015, 2017; Wanner et al., 2018b) and has also been observed in fractured rock (e.g., Schaefer et al., 2018). Some numerical studies of back-diffusion have been carried out to demonstrate this phenomenon. Parker et al. (2008) used two numerical models to illustrate the manner in which a contaminant can diffuse into a thin low-permeability unit and subsequently back-diffuse into an underlying and an overlying aquifer, although the study did not include degradation processes. Seyedabbasi et al. (2012) also looked specifically at diffusive processes using a multiple aquitard lens configuration. Wanner et al. (2018b) included degradation in a two-layer model, testing three spatially-dependent degradation configurations. While these studies have provided important illustrations of the phenomenon of back-diffusion, to date, no study has thoroughly explored the relative influences of advection, diffusion, sorption, and degradation on plume persistence.

In general, advection tends to be the dominant mechanism for contaminant transport in aquifers while diffusion is the dominant mechanism in aquitards. In a given hydrogeological unit, the relative importance of these two transport mechanisms can be described by the dimensionless Péclet number, although the definition of this number in the context of subsurface transport is open for debate (Huysmans and Dassargues, 2005). These processes also contribute to determining the proportion of the contaminant that will enter a unit where degradation can occur.

Most contaminants and other solutes adsorb to some degree in low-permeability media where specific surface area is very large and organic content may be specific. Sorption has the primary effect of slowing the plume due to the temporary "storage" of a portion of the chemical species in its adsorbed form (Allen-King et al., 1995). The strength of this effect can be quantified through the retardation factor or adsorption coefficient. A potentially significant side-effect of sorption dynamics is increased degradation as the residence time of each solute molecule in an aquitard is increased, possibly leading to lower peak concentrations down-gradient.

Degradation of several contaminants, notably including chlorinated hydrocarbons (CHCs) such as trichloroethene (TCE), has been observed to occur in aquitards (Wanner et al., 2016). This degradation can occur via several mechanisms (e.g., Hunkeler et al., 2005; Badin et al., 2014; Cretnik et al., 2013; Wanner et al., 2018a) and can occur at a large range of rates (e.g, Lu et al., 2006; Wanner et al., 2016). Both abiotic and biotic degradation pathways are possible for many contaminants (Zimmermann et al., 2020).

It is the interplay between degradation and the transport processes of advection, diffusion, and sorption that determines the duration of plume persistence. Other aspects of contaminant fate such as the maximum concentration observed at a given point are similarly affected by the complex relationships between these processes. The relative degrees to which degradation, transport processes, and physical configurations affect the dynamics of groundwater contaminant plumes is of significant interest because of their importance in informing remediation and management decisions.

Understanding the relative importance of various processes is vital for making assessments of contaminant fate. Here, we present the first study of the advective, diffusive, sorptive, and reactive parameters that govern contaminant fate in layered sedimentary systems with contrasting high and low hydraulic conductivity layers. To maximise the applicability of this approach, as well as the utility of the information, we vary several parameters over realistic ranges to quantify their influence on both absolute concentration and plume persistence. We also reduce the dimensionality of the parameter space and identify trends and limits in persistence based on novel combined parameters. Specific regimes under which advective flow velocity dominates as a plume persistence control are similarly defined. While we take inspiration from current knowledge of selected well-known contaminants such as CHCs, we note the broad applicability of the analysis here to other aqueous-phase contaminants and solutes.

2. Theory and numerical modelling

2.1. Contaminant transport

Aqueous-phase groundwater contaminants originate in source zones where they may be present as dense non-aqueous phase liquids (DNAPLs) or as concentrated aqueous-phase chemicals. The original source can be leaky containers or contaminants directly present in the pore space. Regardless of the origin of an aqueous-phase contaminant plume, a subsurface source zone can generally be delimited (e.g. Falta et al., 2005; Wanner et al., 2017). Once dissolved into the aqueous phase, transport of contaminants is governed by the mass balance equation, also known by other names such as the advection-dispersion-reaction-sorption equation or scalar transport equation:

$$\frac{\partial (C)}{\partial t} = \frac{1}{f_{re}}\left[\nabla \cdot (D\nabla C) - \nabla\left(C\vec{v}\right)\right] + R + Q \tag{1}$$

where C is the concentration in the pore space of a given chemical species [SI units: mol/m^3]; f_{re}, the retardation factor [1]; D, the hydrodynamic diffusion/dispersion coefficient [m^2/s]; $\vec{v}$, the groundwater velocity [m/s]; R, a reaction term [mol/m^{3}s]; and Q, a source/sink term [mol/m^{3}s]. Eq. (1) is valid for a porous material with homogeneous porosity.

Advection is the transport of a solute via the flow of water in the subsurface due to a hydraulic (pressure) gradient. The advective term in Eq. (1), $\nabla\left(C\vec{v}\right)$ is presented in its conservative form, although it is often written as $\vec{v} \cdot \nabla C$ if this term dominates $C\nabla \cdot \vec{v}$ in the domain due to relatively uniform flow. The advective velocity of groundwater can be evaluated as:

$$\vec{v} = \frac{\vec{q}}{\epsilon} = \frac{1}{\epsilon} K \nabla H \tag{2}$$

where K denotes hydraulic conductivity [m/s]; ϵ, porosity [1]; H, hydraulic head [m]; and $\vec{q}$, the Darcy velocity [m/s]. Diffusion is the transport of a solute due to the concentration gradient. Dispersion is transport of a solute due to heterogeneity of the porespace and is dependent on velocity. The dispersion/diffusion coefficient can be defined as:

$$D = D_e + \vec{\alpha} \mid v \mid \tag{3}$$

where D_e is the effective diffusion coefficient and α is dispersivity [m]. In two- or three-dimensional systems, dispersivity is generally a vector reflecting anisotropy as dispersion is generally much greater in the

direction of advective flow (Gelhar et al., 1992). The diffusion component is a function of both the porous material and the solute-solvent mixture properties. Effective diffusivity can be modelled as:

$$D_e = D_F \frac{\epsilon}{\tau} \tag{4}$$

where D_F is the fluid diffusion coefficient for a given solute in water; ϵ is the porosity; τ is the tortuosity. Tortuosity can, in turn, be approximated by the Millington and Quirk (1961) model:

$$\tau = \epsilon^{-1/3} \tag{5}$$

In situations where $v \ll D_F/\alpha$, a situation generally true in low permeability units, dispersion will be negligible. Conversely, if $v \gg D_F/\alpha$, dispersion will play a more important role than diffusion.

In Eq. (1), the terms R and Q indicate sinks and sources, both of which may vary spatially and temporally. In the context of our present study, the sinks are degradation reactions for the aqueous-phase contaminant of interest. Likewise, sources are the introduction of a given molar flux or fixed concentration into the domain of interest. Degradation of contaminants such as CHCs has been observed to be significant in low permeability units and insignificant in aquifers (Takeuchi et al., 2011; Wanner et al., 2016). In the aquitard, the reaction term can be modelled as a first-order degradation reaction:

$$R = -r_1 C \tag{6}$$

where r_1 is the first-order reaction constant. While non-linear reaction kinetics are also possible, the scope of this study is limited to first-order degradation reactions.

A final consideration for the transport of aqueous-phase contaminants or other solids is sorption, which involves individual molecules adsorbing to, and desorbing from, pore surfaces. Sorption processes have the effect of slowing the transport of a solute with respect to that of water. When this occurs in a reactive unit, it can enhance contaminant degradation (Smith et al., 2009; Damgaard et al., 2013). Under a linear sorption isotherm regime the amount of solute adsorbed is directly proportional to the concentration of the solute:

$$C_{\text{ads}} = K_{\text{ads}} C \tag{7}$$

where C_{ads} is the concentration of the adsorbed species and K_{ads} is the adsorption constant. Here, the effect of adsorption will manifest itself in the governing transport equation as the retardation factor:

$$f_{re} = 1 + \frac{\rho_b}{\varepsilon} K_{\text{ads}} \tag{8}$$

where ρ_b is the bulk density.

2.2. Numerical modelling

Three general situations are investigated in this study (Fig. 1):

- aquifer between aquitards, contaminant source removed after fixed time (Scenario A);
- aquitard between aquifers, contaminant source removed after fixed time (Scenario B); and
- aquifer between aquitards, constant contaminant source (Scenario C).

Scenarios A and B involve a constant concentration contaminant source which is removed after 10 years. This is studied for the case of an aquifer overlain and underlain by aquitards and for the case of an aquitard overlain and underlain by aquifers. An additional configuration (Scenario C) of an aquifer between two aquitards with no source removal is also studied.

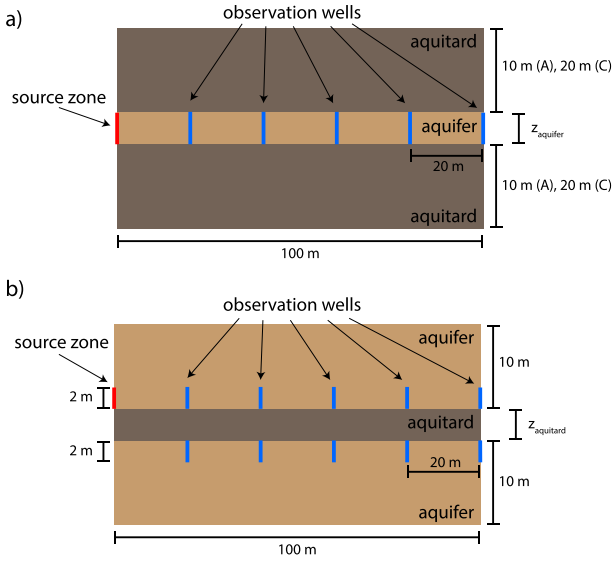

Fig. 1. Schematic diagrams of the investigated scenarios: (*a*) Scenarios A and C, (*b*) Scenario B. There is a hydraulic head difference of 1 m from the left side to the right side of the entire domain in each Scenario. Flow is thus left-to-right. The analysis carried out in this work focuses on the observation wells at 100 m from the source (see Appendix A).

The general approach employed here involves executing numerical models multiple times with different combinations of parameters and subsequently analysing the ensemble of the results. This methodology has previously been used to determine the relative significance of different controls on hydrological phenomena. For example, Cardenas and Wilson (2007) investigated the influence of permeability and flow characteristics on streambed thermal regimes, while Carlier et al. (2019) looked at geological, topographical and meteorological controls on streamflow. This approach provides fundamental information about the relative influences of parameters on outcomes, but requires a degree of simplification so that the study remains relatively tractable and general. Properties in the individual units are homogeneous and thus heterogeneity-induced mixing (e.g. Cirpka et al., 1999; Werth et al., 2006) is not considered. The numerical models are implemented and executed using *COMSOL Multiphysics* (COMSOL AB, 2019) which provides a powerful finite element solver and parameter sweep tools and enables fully customisable evaluation of reactive transport in porous media (e.g., Nardi et al., 2014; Lippmann-Pipke et al., 2017; Halloran et al., 2019).

2.2.1. Plume persistence after remediation

In Scenarios A and B, an aqueous-phase contaminant is introduced as a constant concentration boundary condition from years 0–10 (Fig. 1). As the flow rate is constant each model, this is equivalent to a constant flux boundary condition. In Scenario A, the source zone spans the entire aquifer. In Scenario B, the source zone spans 2 m directly above the aquitard. In both models, there is a hydraulic head difference of 1 m from the left to the right side of the modelled domain. The initial concentration of the solute throughout the model domain is 0. Dirichlet boundary conditions are implemented at the source zones as fixed concentrations during 10 years, with a 0.25 year continuous second-derivative ramp-up and ramp-down to ensure numerical stability. Dirichlet boundary conditions of zero concentration are implemented at the left boundary for non-source zones. Neuman boundary conditions ($\hat{x} \cdot \nabla C = 0$) are implemented for the right boundary, while no-flow conditions are implemented at the top and bottom boundaries. First-order reactions (Eq. (6)) occur in the aquitard layers. The numerical models were meshed with non-uniform rectangles. A higher concentration of nodes is defined at the left of the model, as well as in the aquitard near the interface and the aquifer (Scenario A) and in the aquifer near the interface and the aquitard (Scenario B). This results in between 6000 and 9380 elements for the entire domain

in the different configurations. The models are executed for 210 years, i.e., 200 after the removal of the contaminant source.

Observation wells are implemented as line averages, which correspond to groundwater samples from wells screened at the defined depth ranges (Fig. 1). In Scenario A, the wells span the entire thickness of the aquifer, while in Scenario B, they span the 2 m directly above and below the aquitard. These observation wells are implemented at 20, 40, 60, 80 and 100 m from the source location, resulting in five sampling locations for Scenario A and ten for Scenario B. The results at the different observation wells are qualitatively similar, exhibiting a rise to a maximum concentration value, followed by a decay in concentration. Due to these similarities and the limited space for presenting results, the primary focus here is on the results at 100 m (see Appendix A for information on other locations).

In order to model reactive transport of a solute in porous media, many parameters must be defined. The goal of this work is to investigate various controls on contaminant persistence via these parameters in selected configurations, all while remaining as general as possible. Nonetheless, practical choices need to be made with respect to the parameters investigated and the values chosen. We have selected five parameters whose values are varied in individual executions of the model. In each of these scenarios, the thickness of the bounded unit (z_a), the fluid diffusion coefficient (D_F), the degradation reaction constant (r_1), the aquifer hydraulic conductivity (K_{aquifer}), and the retardation factor (f_{re}) are varied over a range of values relevant for a variety of contaminants (and other solutes) in sedimentary hydrogeological systems (Table 1). These parameters are assigned values which are scaled logarithmically over the selected range. Here, the models are executed for every possible combination of these parameters values.

The number of combinations of parameters investigated is 96 for each aquifer (Scenario A) or aquitard (Scenario B) thickness, which results in 288 model executions for each scenario. Other parameters are fixed at values that are representative of sandy aquifers or clayey aquitards (Table 1). In both scenarios, the hydraulic gradient is fixed at 0.01. The resultant range of horizontal advective velocities in the aquifer (5.71–143×10^{-8} m/s) and in the aquitard (2.5×10^{-12} m/s) allows us to calculate the total range of Péclet numbers investigated using the definition:

$$Pé = \frac{L_c v_x}{D_e} \tag{9}$$

where L_c is the characteristic length. This is taken here to be 100 m as the analysis in this study focuses on results at 100 m from the source (see Appendix A), although it must be noted that care should be taken so as to not blindly interpret Péclet numbers as several definitions exist (Huysmans and Dassargues, 2005). Combining Eqs. (2), (4), and (5) with Eq. (9), we obtain:

$$Pé = \frac{L_c \frac{dH}{dx} K}{D_F \epsilon^{7/3}} \tag{10}$$

By this definition, the resultant Péclet numbers range between 0.395 and 3.95 for the aquitard and 1.07×10^4 – 2.69×10^6 in the aquifer, indicating relative diffusion dominance in the aquitard and advection dominance in the aquifer.

2.2.2. Constant source

Scenario C (Fig. 1a) is similar to Scenario A, except that contaminant source is never removed. Additionally, the model is executed for 1000 years and the aquitard layers extend 20 m above and below the aquifer layer. This ensures that negligible concentrations are observed at the upper and lower boundaries of the model domain. The fixed concentration boundary condition is constant for the entire duration of the model runs. Additionally, rather than exporting yearly data as in the source removal scenarios, results from the models in this scenario are exported at 5-yearly intervals for the first 100 years, followed by 20 year increments.

3. Results and discussion

3.1. Procedure for analysis

The raw concentration time-series results of all varied parameter combinations (Table 1) are exported from the numerical model and subsequently merged. Processing of the data is carried out using *python* (see Appendix A for details). Data for the source-removal scenarios (Fig. 1) is analysed to determine (Fig. 2):

- C'_{max}, the peak normalised concentration value at the observation well;
- t_{att}, the time required for the concentration at the observation well to be attenuated by a given factor after the concentration peak;
- and, equivalently, $n_{v,att}$, the number of pore volumes required for the concentration at the observation well to be attenuated by a given factor

Table 1
Values of varied and fixed parameters in the investigated scenarios.

	Symbol	Value(s)
	Varied parameters	
Aquifer or aquitard thickness	$z_a = z_{\text{aquifer}}$ or z_{aquitard}	0.2, 1, 5 m
Fluid diffusion coefficient of solute	D_F	0.215, 4.64, 1, 2.15×10^{-9} m^2/s
First-order reaction constant (in aquitard)	r_1	0.01, 0.1, 1, 10/year
Hydraulic conductivity (aquifer)	K_{aquifer}	0.2, 1, 5×10^{-5} m/s
Horizontal advective velocity (in aquifer)[a]	$v_x = \frac{1}{\epsilon} K_{\text{aquifer}} \frac{dH}{dx}$	0.0572, 0.286, 1.43×10^{-6} m/s
Retardation factor	f_{re}	1.35, 3.5[b]
	Fixed parameters	
Horizontal hydraulic gradient	$\frac{dH}{dx}$	0.01
Porosity of the aquifer	$\epsilon_{\text{aquifer}}$	0.35[c]
Porosity of the aquitard	$\epsilon_{\text{aquitard}}$	0.4[c]
Dispersivity	α	0.45 m (horizontal), 0.0005 (vertical)[d]
Tortuosity	τ	$\varepsilon^{-1/3}$[e]
Hydraulic conductivity (aquitard)	K_{aquitard}	1×10^{-10} m/s

[a] Not independently varied, function of K_{aquifer}.
[b] Lower value, e.g., ethene, Thouement et al. (2019); Higher value, e.g., TCE, Parker et al. (2008); Carey et al. (2015).
[c] e.g., Parker et al. (2008); Carey et al. (2015).
[d] e.g., Gelhar et al. (1992); Jensen et al. (1993).
[e] Millington and Quirk (1961).

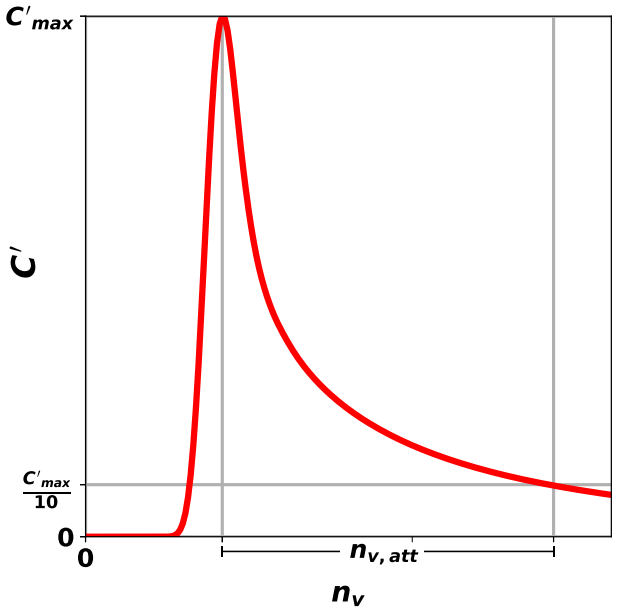

Fig. 2. General example of a normalised concentration C' time-series as a function of the number of pore volumes n_v. The definitions of C'_{max} (Figs. 3 and 4) and $n_{v,att}$ (Figs. 6 and 7) are indicated. Conversion between time and number of pore volumes is calculated by Eq. (11).

As the numerical model results are exported at yearly intervals, sub-annual temporal precision is gained by making a linear approximation in the time step wherein the concentration falls below the specified threshold. Conversion between time and number of pore volumes is calculated by:

$$n_v = v\frac{t}{x} = \frac{tK_{\text{aquifer}}\dfrac{dH}{dx}}{\epsilon_{\text{aquifer}}x} \tag{11}$$

where x here is the horizontal distance between the source and the observation well.

For clarity, we restrict analysis here to the wells at 100 m from the source (see Appendix A). We also focus on an attenuation factor of 0.1 (Fig. 2), meaning that we calculate the time and pore volumes required for the concentration to drop to a tenth of the maximum value. Additionally, to avoid analysing numerical noise, we eliminate cases where the maximum concentration at the observation well never exceeds 1×10^{-5} of the input concentration, which is equal to the solver tolerance in the models.

For the constant-source case, analysis is carried out slightly differently. Here, the primary interest is the spatial extent of the plume at equilibrium conditions. To determine the spatial extent of a constant-source plume, least-squares fits of the normalised equilibrium concentration, C'_{eq}, at the source ($C'_{eq} = 1$), and at the five observation wells are performed using an exponential decay equation:

$$C'_{eq}(x) = e^{-x/x_0} \tag{12}$$

where x_0 is a measure of plume extent. Specifically, it is the distance at which the contaminant concentration a hypothetical observation well will reach $1/e$ (0.368) of the source concentration.

As five parameters (r_1 takes 4 values; D_f, 4; K_{aquifer}, 3; z_a, 3; and f_{re}, 2) are varied in this investigation, concise visualization of the multi-dimensional parameter space requires a *plots-of-plots* approach. The results are thus visualised as colour-coded matrices with values explicitly labelled. A separate matrix of results for each of the two retardation factors investigated is presented.

3.2. Concentration maxima and equilibria

In the context of legal concentration limits of a given compound, the maximum concentration of a contaminant at a given location down-gradient from a source zone is an important concern for the management of contaminated sites. In Scenario A, the maximum concentration observed at the observation well 100 m from the source (Fig. 3) varies significantly depending on the values of the parameters. At the extremes, values $<1 \times 10^{-5}$ occur at lower K_{aquifer} values and smaller aquifer thickness, while a maximum of 0.984 is observed at high z_a and K_{aquifer} and low r_1, D_F, and f_{re} where the configuration approaches plug flow-like behaviour.

In Scenario B, the maximum concentration at the observation well 100 m from the source (Fig. 4) varies over a smaller range for the investigated parameter combinations. Here, the extreme values are 0.021 and 0.479. These occur at the same parameter extremes as in Scenario A, although the influence of z_a has the opposite trend as in Scenario A at high r_1. Analysis of the results for the observation well below the aquitard is not presented here (see Appendix A), but we note that the maximum value there is 0.139 for $r_1 = 0.1$/a, $D_F = 2.15 \times 10^{-9}$ m^2/s, $z_{\text{aquitard}} = 0.2$ m, $f_{re} = 1.35$, and $K_{\text{aquitard}} = 1 \times 10^{-5}$ m/s.

For each parameter, a trend in maximum concentration occurs. In general, higher aquifer hydraulic conductivities, lower reaction rates, lower fluid diffusion constants, lower retardation factors, and, in Scenario A, higher aquifer thicknesses lead to higher maximum concentrations. Taken individually, each of these trends has a physical explanation. For example, a higher retardation factor will result in longer residence times in the reactive aquitard layer, leading to a higher probability of degradation for a given molecule and thus lower concentrations down-gradient. The ensemble effects of the multiple factors and their relative importances, however, are not immediately obvious through these types of simple thought-experiments. A phenomenon of note is that of the relative insensitivity, in most parameter combinations, of the maximum concentration to the reaction rate which is varied over three orders of magnitude. For Scenario B, it appears that diffusion plays a more important role than degradation in governing the maximum concentration at the observation well.

In Scenario A (Fig. 3), there is significant sensitivity to the thickness of the aquifer layer. In a thin aquifer layer, a given molecule of the solute has a greater probability to enter a reactive aquitard layer where it may be degraded before arriving at the right side of the domain. In Scenario B (Fig. 4), there is little sensitivity to the aquitard layer thickness. This is due to the fact that the portion of the contaminant that diffuses into the aquitard layer and subsequently back-diffuses into the aquifer layer to contribute to the maximum concentration will not penetrate very deep into the aquitard layer. While certain parameters may not have a significant effect on the maximum concentration down-gradient from the source, they can contribute to increased or decreased persistence of the contaminant through various mechanisms.

Finally, for the constant source case (Scenario C), the equilibrium concentrations (Fig. 5) are determined as described in Section 3.1. The trends in equilibrium concentration are unsurprisingly similar to those of the maximum concentration in Scenario A. However, for the constant-source case, the reaction rate appears to play a stronger role in determining the concentration at the observation well. Additionally, the influence of aquifer hydraulic conductivity appears to be less pronounced. These factors are due, in part, to this analysis of Scenario C being effectively steady-state, while Scenario A is transient.

3.3. Persistence

Temporal aspects of contaminant transport are often highly uncertain. While back-diffusion is know to contribute to plume persistence, the relative importance of advection, diffusion, sorption, and degradation on the temporal dynamics of a plume are not generally self-

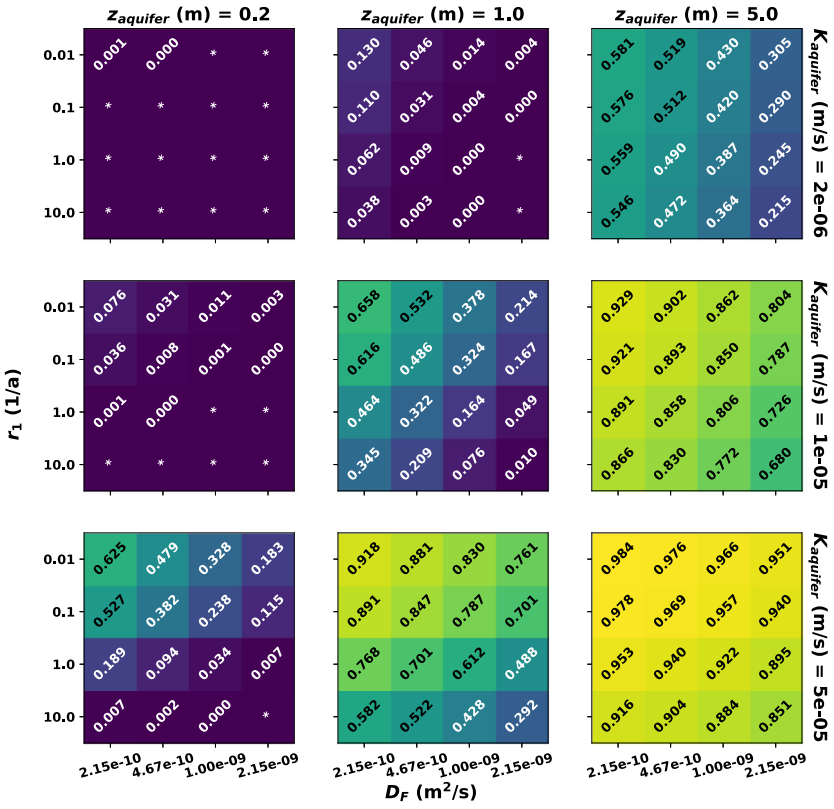

(a) $f_{re} = 1.35$

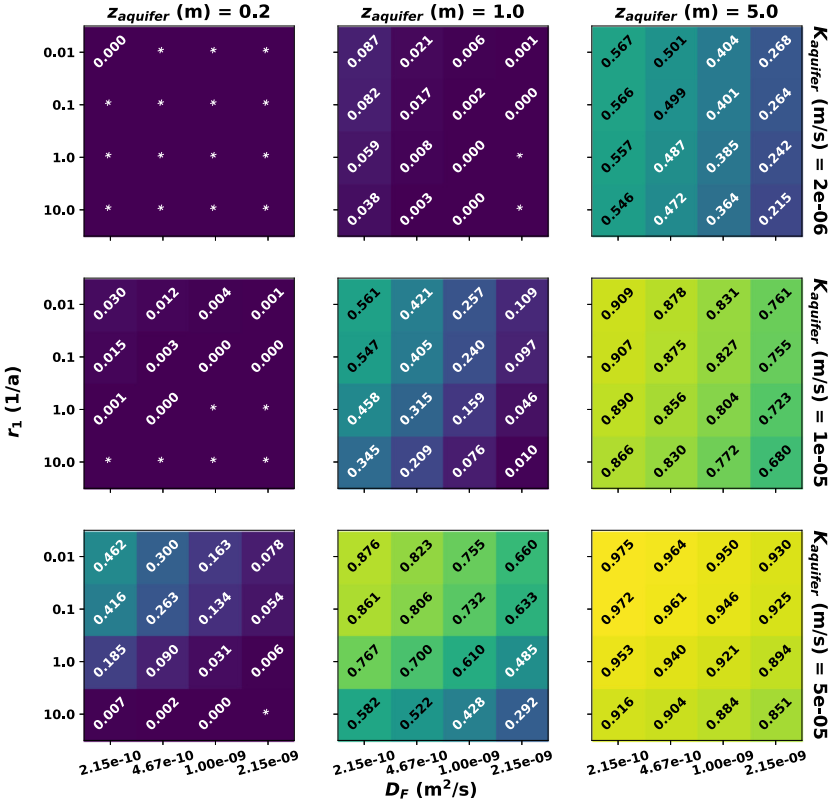

(b) $f_{re} = 3.5$

evident at a given site (Chapman and Parker, 2005; Parker et al., 2008; Yang et al., 2017; Wanner et al., 2018b).

In Scenario A, between 0.20 and 70.36 pore volumes are required for the normalised concentration at 100 m to be attenuated by to 1/10 of C'_{max} (Fig. 6). Values higher than 70.36 may occur for certain cases where only a minimum bound was determined. This large variability shows the influence of the various controls. It is evident that the thickness of the aquifer layer plays an important role. For the thickest aquifer layer (z_a=5 m), the other four investigated parameters have very little influence on the relatively short duration of persistence ($n_{v,att}$ ranges between 0.23 and 1.35) due to the smaller proportion of the contaminant that enters the aquitard layers. At higher reaction rates (r_1), the influence of sorption through the retardation factor (f_{re}) appears to be negligible. At lower reaction rates, however, there can be a significant increase in plume persistence due to increased sorption. This is due higher f_{re} resulting in longer residence times in the aquitard layers, which, when degradation is limited, causes a longer duration of back-diffusion.

In Scenario B, persistence varies much less than in Scenario A. For all parameter combinations explored, between 0.22 and 2.73 pore volumes are required for the concentration at the investigated observation well to drop by a factor of 10 (Fig. 7). For the observation well below the aquitard layer, at 100 m from the source (Fig. 1), $n_{v,att}$ ranges between 0.22 and >90 (see Appendix A), with thicker aquitard layers resulting in longer persistence but lower C'_{max}. For z_a=5 m, in the extreme cases of low f_{re}, low $K_{aquifer}$, low r_1, and high D_F (see Table 1), C'_{max} only reaches a value of ~0.001, thus the model can be considered nearly equivalent to an infinite two-layer model.

As scenarios A and B were executed for 200 years after source removal, only a minimum t_{att} of 200 years can be established for cases where the normalised concentration did not drop below 1/10 of C'_{max}. Thus, when presented in terms of $n_{v,att}$, 200 years corresponds to 3.62, 18.1, and 90.6 pore volumes for $K_{aquifer} = 2 \times 10^{-6}$, 1×10^{-5}, and 5×10^{-5} m/s, respectively (Eq. (11)). Cases where attenuation by the specified factor is not observed within the duration of the model runs tend to be those with small C'_{max} (<0.03). The upper bound of the relationship between the maximum concentration at an observation well and the number of pore volumes required to attenuate the concentration by a given amount (Fig. 8) appears to be inverse. This is due, primarily, to the interplay between diffusive and advective transport. In this figure, cases with high reaction rate constants tend to be well below the upper limit due to increased degradation of the proportion of the compound that diffuses into the aquitard. Furthermore, a relationship between the thickness of the aquifer layer and both C'_{max} and $n_{v,att}$ exists. Thin aquifer layers overlain and underlain by reactive low-permeability units will see weaker concentrations at observation wells, but those concentrations will persist for longer.

3.4. Plume length at equilibrium

The spatial extent of a plume under competing advective, reactive, diffusive, and sorptive processes is a key concern when evaluating any contaminated site. These various processes, as well as spatial factors, can have very pronounced effects on plume extent. For the ranges of parameters explored here, the spatial extent of a plume at equilibrium, as measured by the parameter x_0 (Eq. (12)) in Scenario C, varies between <1 m and >14 km (Fig. 9). Sorption plays little role as it will primarily serve to delay the establishment of equilibrium conditions, but do little to change them. All other parameters have significant effects on the spatial extent of a plume.

The hydraulic conductivity of the aquifer layer ($K_{aquifer}$) and, correspondingly, the horizontal advective velocity (v_x), play an obvious role in determining the length of a plume. At low reaction rates, its effect on x_0 is nearly linear. However, at higher reaction rates an increase in $K_{aquifer}$ by a given factor causes a smaller increase in x_0. The influence of z_a is very pronounced as it influences the proportion of the contaminant that will enter the reactive aquitard layers. The first order reaction constant (r_1), which varies by three orders of magnitude in our study, has a lesser effect on plume persistence, particularly for thicker aquifer layers. The effect of diffusion is also less pronounced and is weakest for thicker aquifer layers and higher hydraulic conductivity.

3.5. Dimensionality reduction

Dimensionality reduction allows for the construction of combined parameters that can potentially reveal trends, regimes in which certain processes dominate, or limits on plume behaviour. In order to determine a parameter-space with reduced dimensionality, we employ two approaches - one with an explicit physical basis and another using Buckingham Pi-theory. For the physical basis approach, we look separately at the processes occurring in the aquifer and aquitard. Noting that, at equilibrium, if first-order reactions (Eq. (6)) occur uniformly in an aquitard that is bounded by a constant concentration C_0 at its upper boundary, then Eq. (1) can be simplified to obtain a form of the diffusion-reaction equation:

$$0 = D_e \frac{\partial^2 C}{\partial z^2} - r_1 C \tag{13}$$

which has the solution

$$C = C_0 e^{\pm \sqrt{\frac{r_1}{D_e}} z} \tag{14}$$

The flux, J, into the aquitard is governed by Fick's law (Fick, 1855):

$$J = D_e \frac{\partial C}{\partial z} \tag{15}$$

which, combined with the positive exponent solution of Eq. (14), gives:

$$J = \sqrt{r_1 D_e} C = \sqrt{r_1 D_e} C_0 e^{-\sqrt{\frac{r_1}{D_e}} z} \tag{16}$$

At the aquifer-aquitard boundary ($z = 0$), this, combined with Eqs. (4) and (5), reduces to:

$$\frac{J}{C_0} = \sqrt{r_1 D_e} = \sqrt{r_1 D_F \left(\epsilon_{aquitard}\right)^{4/3}} \tag{17}$$

As transport in the aquifer also plays a role in the dynamics of plume behaviour, we note that the relative proportion of the contaminant that enters the reactive low-permeability layer will be inversely proportional to the thickness of the aquifer z_a. It will also be proportional to residence time in the aquifer and thus inversely proportional to $K_{aquifer}$. Combining these considerations of aquifer and aquitard processes, we arrive at the following constructed parameter:

$$\eta = \frac{\sqrt{r_1 D_e}}{z_a K_{aquifer}} = \frac{\sqrt{r_1 D_F \left(\epsilon_{aquitard}\right)^{4/3}}}{z_a K_{aquifer}} \tag{18}$$

As five parameters are varied in this study, η provides a physical basis for reducing the dimensionality of the parameter space to further assist in identifying potential trends, regimes, and limits.

Fig. 3. Maximum normalised concentrations, C'_{max}, observed at observation well 100 m from source for the aquifer between aquitards source-removal case (Scenario A). Asterisks denote cases where the normalised concentration did not exceed a specified cutoff (1×10^{-5}).

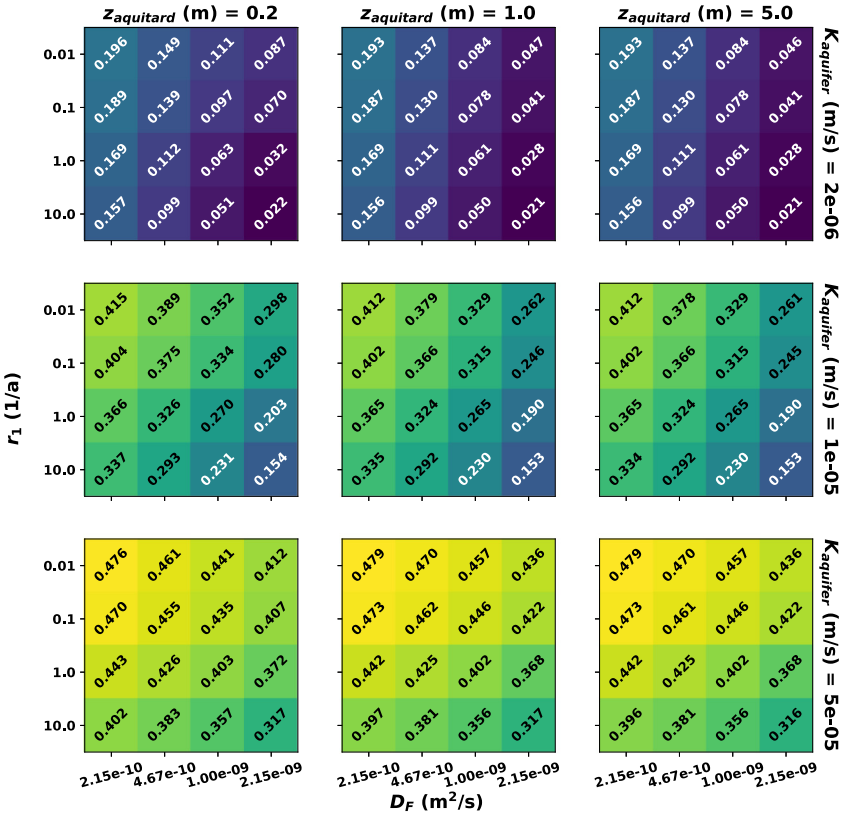

(a) $f_{re} = 1.35$

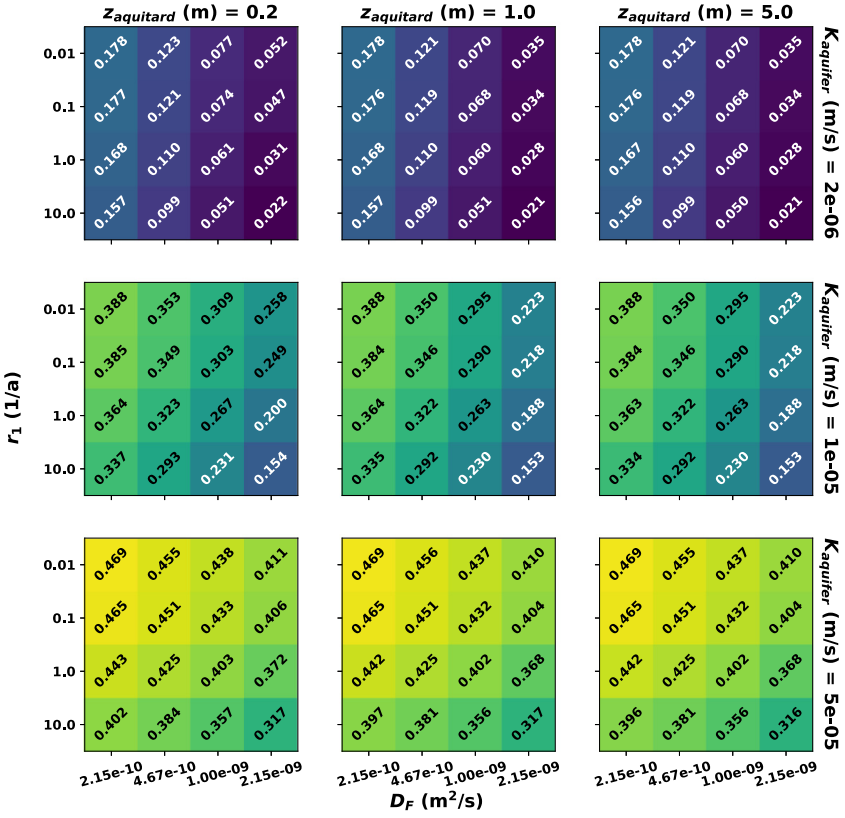

(b) $f_{re} = 3.5$

Fig. 4. Maximum normalised concentrations, C'_{max}, observed at observation well 100 m from source (*above* aquitard layer) for the aquitard between aquifer source-removal case (Scenario B).

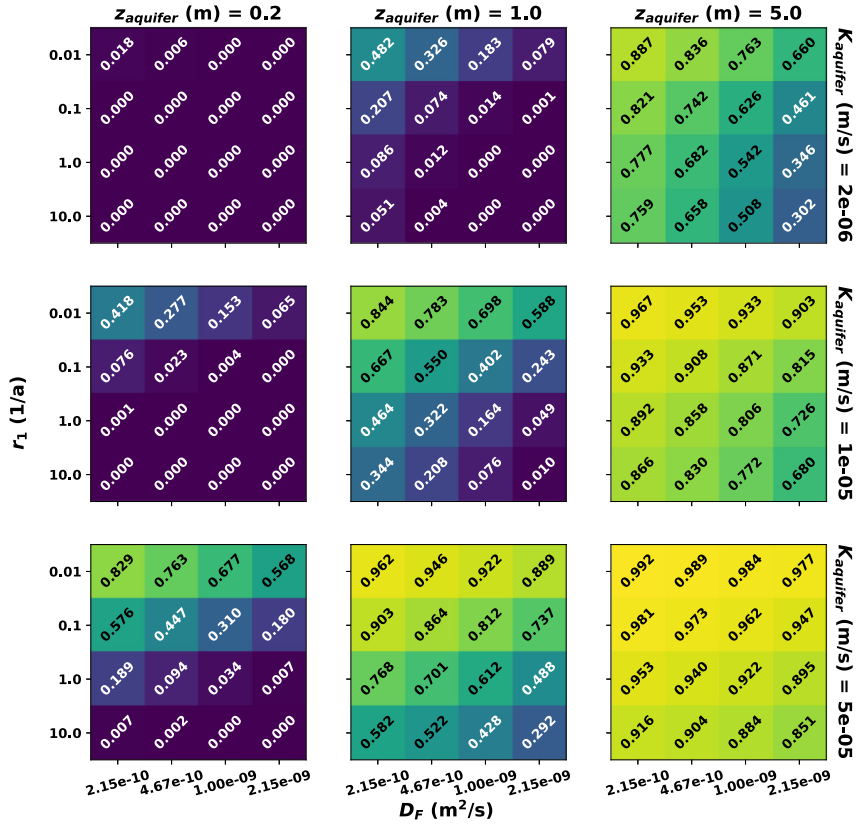

(a) $f_{re} = 1.35$

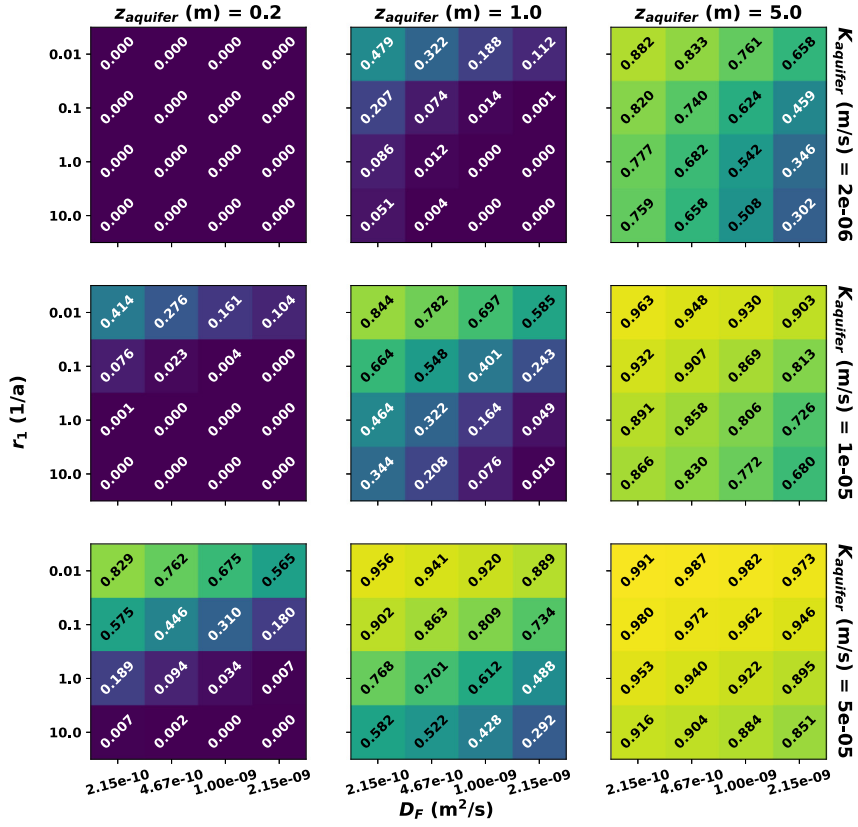

(b) $f_{re} = 3.5$

Fig. 5. Equilibrium normalised concentrations, C'_{eq} for the constant source case (Scenario C) at the observation well 100 m from the source.

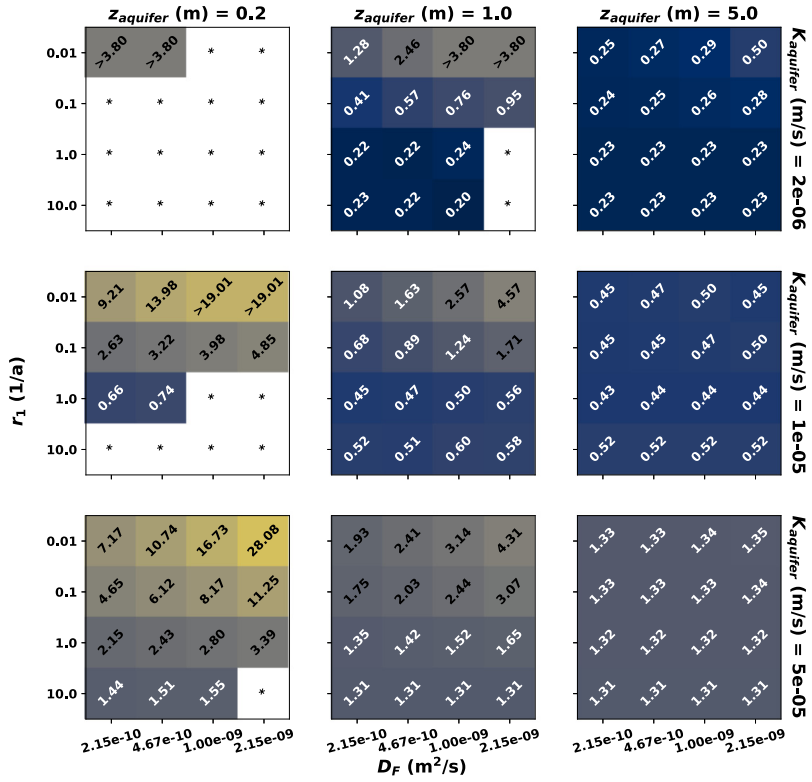

(a) $f_{re} = 1.35$

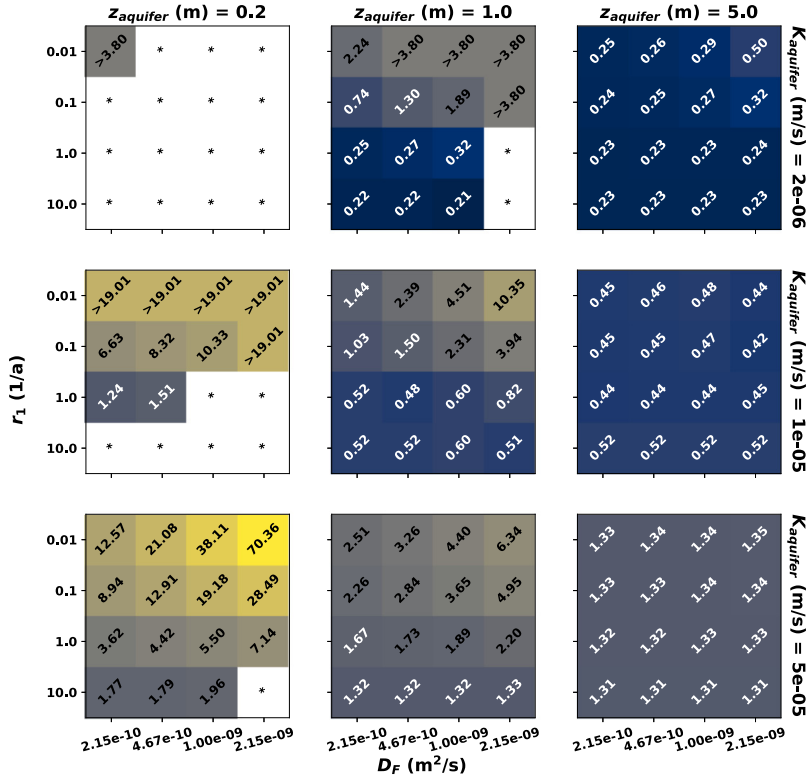

(b) $f_{re} = 3.5$

Fig. 6. $n_{v,att}$ (Eq. (11)) at observation well at 100 m from the source for the aquifer between aquitards source-removal case (Scenario A). Asterisks denote cases where the normalised concentration did not exceed a specified cutoff (1×10^{-5}). To avoid confusion with the C'_{max} data (Figs. 3 and 4 for Scenarios A and B, respectively), a different perceptually uniform sequential colour map (Hunter, 2007) is used for $n_{v,att}$ and, here, it is scaled logarithmically due to the presence of extreme values. Note the cases where only a minimum bound for the $n_{v,att}$ could be determined (those containing a >symbol).

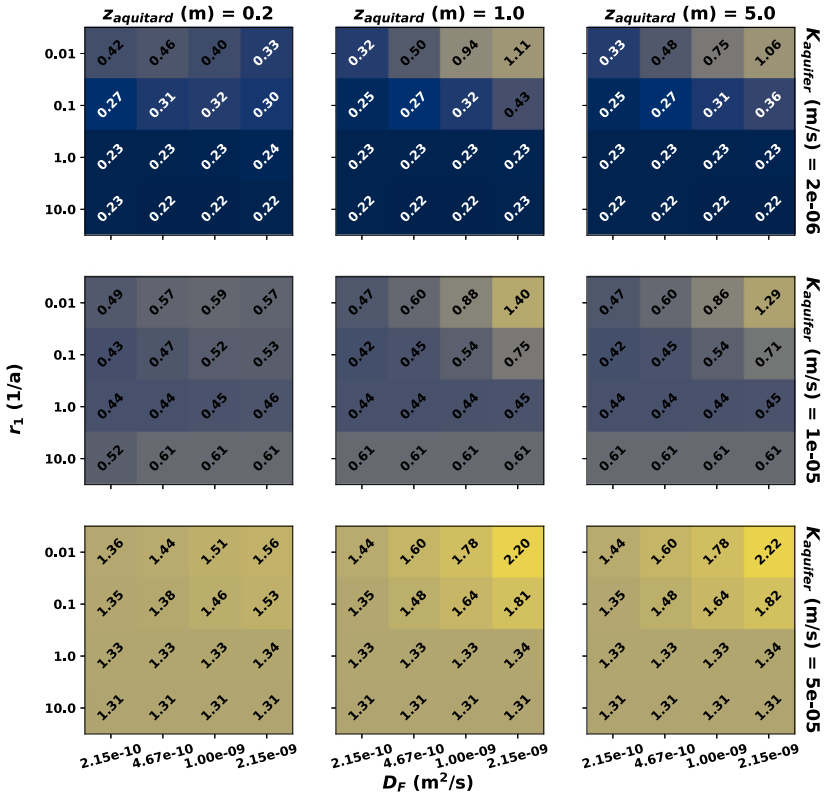

(a) $f_{re} = 1.35$

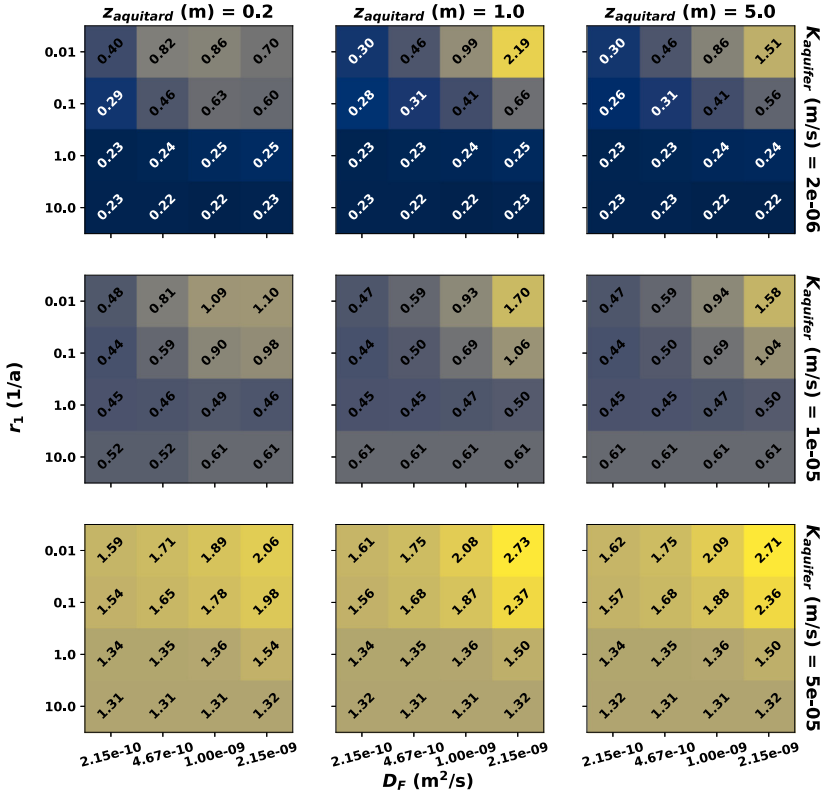

(b) $f_{re} = 3.5$

Fig. 7. $n_{v,att}$ (Eq. (11)) at observation well at 100 m from the source (*above* aquitard layer) for the aquitard between aquifers source-removal case (Scenario B). See caption of Fig. 6 for details.

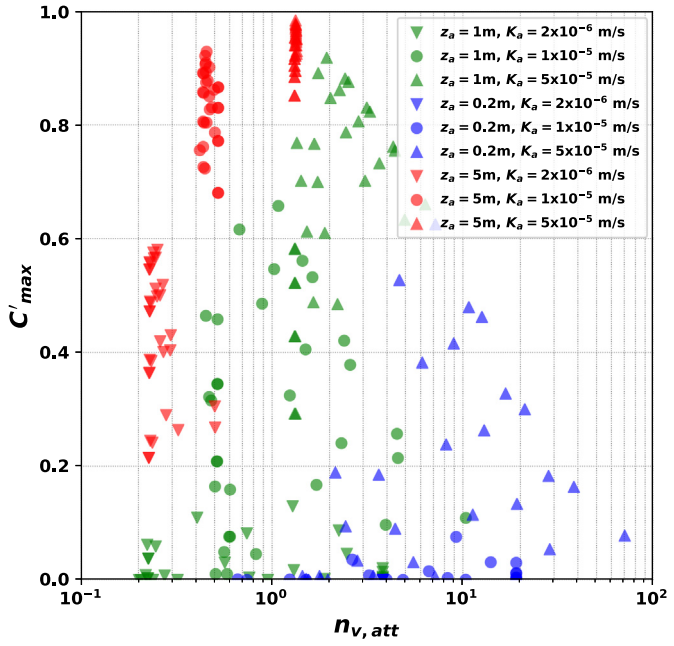

Fig. 8. The relationship between C'_{max} and $n_{v,att}$ for Scenario A (Figs. 3 and 6). The attenuation factor is $\frac{1}{10}$. Values where only the minimum $n_{v,att}$ was determined are not displayed.

A second approach to dimensionality reduction employs Buckingham Pi-theorem (Vaschy, 1892; Buckingham, 1914; Yarin, 2012), also known as the dimensional groups theorem. This theorem provides a basis for physically meaningful dimension reduction from n_p to $n_p - d$ dimensions, where n_p is the number of original parameters and d is the number of fundamental physical dimensions (i.e., time, mass, length, etc.). Following the principles of the Pi-theorem, we can analyse results as functions of dimensionless numbers. Of the five varied parameters, one (f_{re}) is dimensionless. Thus, we have four parameters to which we can apply the theorem: z_a of dimensions $[L]$; D_F or D_e, $[L^2/T]$; r_1, $[1/T]$; and K_{aquifer}, $[L/T]$ (where L and T refer to length and time, respectively). As we have four parameters and two fundamental dimensions, we can form two $(4 - 2{=}2)$ dimensionless groups. Choosing D_e and r_1 as a recurring set (i.e., a set of $n_p - d$ original parameters that cannot, themselves, form a dimensionless group), we obtain the following dimensionless numbers:

$$\Pi_1 = z_a \sqrt{\frac{r_1}{D_e}} \tag{19}$$

and

$$\Pi_2 = K_{aquifer} \frac{\sqrt{D_e}}{r_1^{3/2}}. \tag{20}$$

While the dependencies of the values presented in Figs. 3–7 and 9 on the values of Π_1, Π_2, and η have been investigated, only results with clear trends are presented in Fig. 10. Comparing the attenuation results

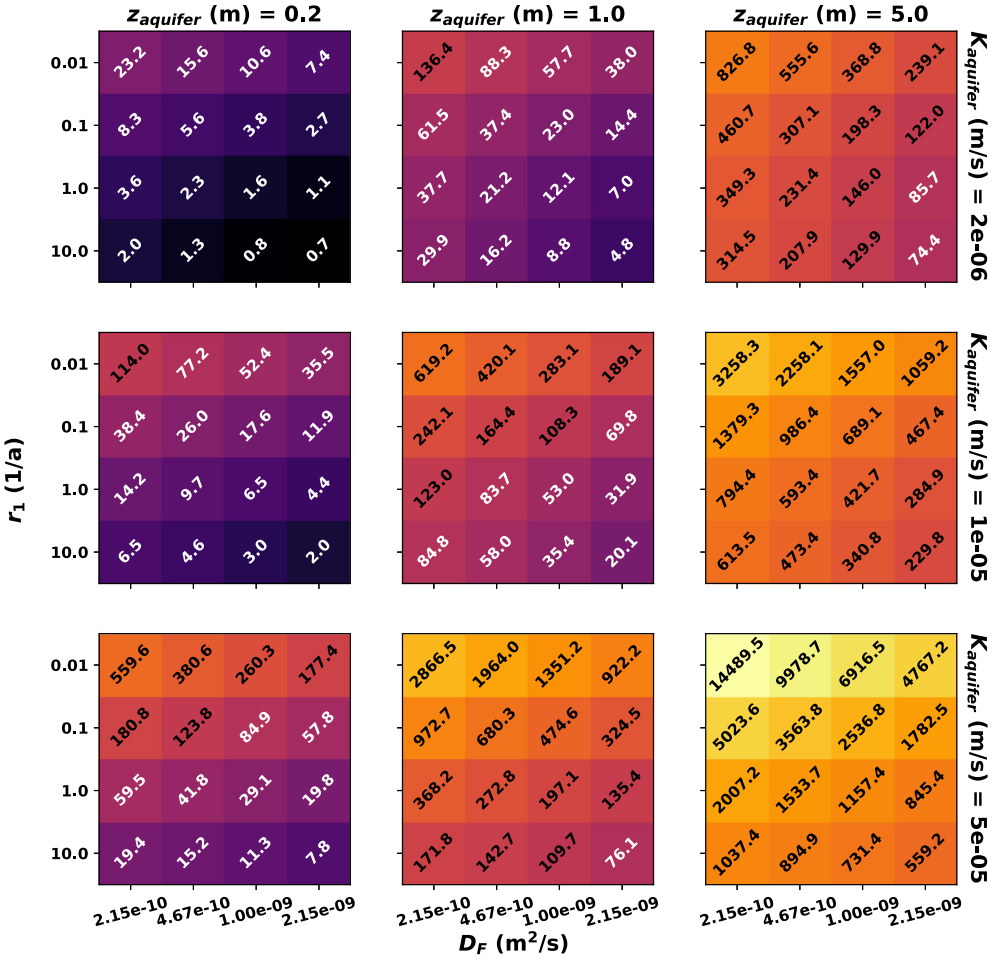

Fig. 9. The spatial decay constant x_0 [m] (Eq. (12)) for Scenario C. Separate figures are not shown for different f_{re} values as retardation factors were observed to have negligible effect in equilibirum conditions. A logarithmically-scaled perceptually uniform sequential colour map is used for x_0.

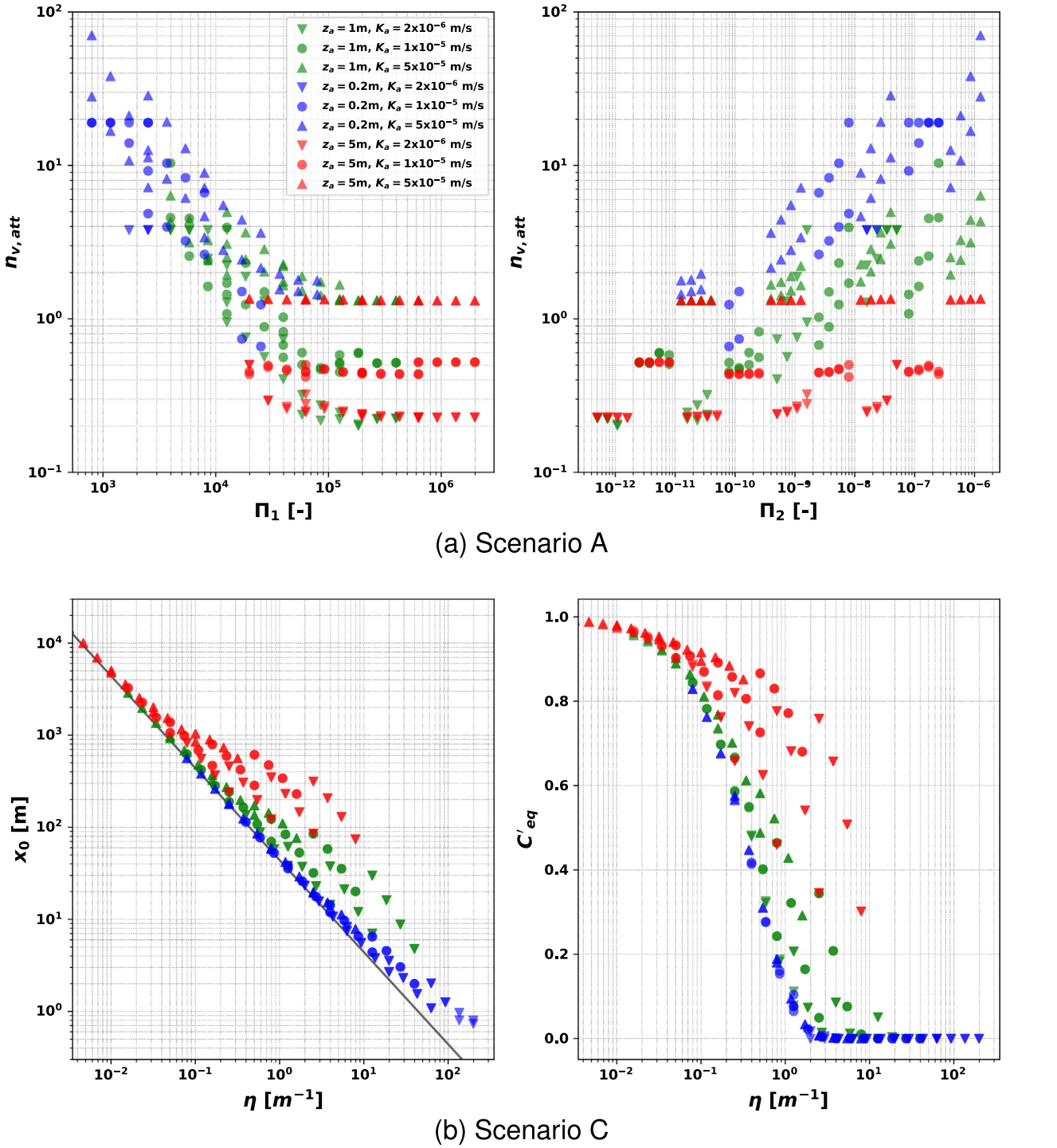

Fig. 10. For Scenario A, $n_{v,att}$ is presented as a function of the constructed parameters Π_1 (Eq. (19)), and Π_2 (Eq. (20)). For Scenario C, the plume length parameter x_0 and the equilibrium concentration C'_{eq} (Eq. (12)) are presented as functions of η (Eq. (18)). The black line (Eq. (21)) delimits the approximate lower bound of the dependence of x_0 on η.

($n_{v,att}$) for Scenario A against Π_1 and Π_2 (Fig. 10a) allows us to identify trends and fundamental limits on plume persistence in a remediation scenario. Below specific values of these constructed parameters, there appear to be fundamental limits on the number of pore volumes required to attenuate the contaminant concentration by a given amount. A clearer limit exists for Π_1 and Π_2. There is a trend toward shorter plume persistence, as measured by $n_{v,att}$, with higher Π_1 and lower Π_2. At $\Pi_1 \gtrsim 10^5$, $n_{v,att}$ is sensitive to the hydraulic conductivity of the aquifer (or, equivalently, the advective flow rate), but has negligible dependence on other parameters. Furthermore, an apparent regime exists for a range of values ($\Pi_1 \lesssim 10^4$) at which the plume will persist for longer than the time required for one pore volume to pass through the domain. For $\Pi_2 \lesssim 10^{-11}$, $n_{v,att}$ values appear bounded by a small upper limit <1. The value of the Π_2 cut-off appears insensitive to the degree of attenuation investigated, while the value of the Π_1 cut-off increases with greater attenuation. For an attenuation factor of, e.g., 100 rather than 10, $n_{v,\,att}$ is only influenced by advection at $\Pi_1 \gtrsim 5 \times 10^5$. For Π_2, however, the value of the $\Pi_2 \lesssim 10^{-11}$ cut-off is unchanged, although the upper bound naturally increases as more time is required for greater attenuation.

For Scenario C, there are no transient effects, and thus clearer relationships between x_0 and η and C'_{eq} and η can be established (Fig. 10b). We recall that η has a physical basis and that it is constructed as a ratio of aquitard processes (degradation and diffusion) to aquifer properties and processes (thickness and advection). It is a measure of the flux into the reactive aquitard layers and includes all of the investigated parameters except sorption which, as discussed earlier, is expected to play a minor role in the equilibrium case. Increasing η results in lower equilibrium concentrations C'_{eq} at a distance downgradient from the source and, similarly, shorter plume lengths as measured by x_0. Indeed, for the relationship between x_0 and η, a lower bound can be clearly established (Fig. 10b):

$$x_0 \geq 44\eta^{-1} \tag{21}$$

This inverse relationship between x_0 and η holds generally for a constant contaminant source in a homogeneous aquifer overlain and underlain by reactive aquitard layers. If another measure of plume extent, such as the distance for the plume to attenuate by a factor $\gamma<1$, is defined (see Eq. (12)), then the right side of Eq. (21) will scale by a factor of $-\ln\gamma$.

Inspecting Eqs. (18)–(20) while observing the trends in Fig. 6, one finds that higher diffusion and lower reaction rates result in longer durations of plume persistence. Diffusion and degradation are represented in all three of these constructed parameters. Smaller aquifer thickness (which appears in Π_1) also causes higher plume persistence. These processes all have fairly straightforward physical explanations, e.g., a thinner aquifer causes a higher proportion of the contaminant to enter the aquitard, leading to greater persistence. The influence of advection through K_{aquifer}, which appears in Π_2, on $n_{v,att}$ is less obvious, which reinforces the usefulness of investigating constructed parameters. Considering $n_{v,att}$ rather than the raw attenuation times allows us to take advection into account. For each of the combinations of parameters investigated in this study, the various controls can have different degrees of influence. The results of Fig. 10 enable the definition of specific regimes under which advection dominates as the controlling mechanism. Even in more spatially complex layered systems, these results provide a powerful basis for initial evaluation based on properties and parameters that can be readily measured or estimated. Nonetheless, caution must be taken in applying these results when, for example, significant heterogeneity is present or when a non-linear degradation reaction regime is in place.

4. Conclusions

The results of this study provide a quantitative assessment of the relative importance of advection, diffusion, sorption, degradation and hydrogeological layer thickness. The values presented here provide valuable information about the relative influences of these controls on maximum concentrations (Figs. 3 and 4), equilibrium concentrations (Fig. 5), plume attenuation times (Figs. 6 and 7), and equilibrium plume extent (Fig. 9). All real sedimentary systems display at least some degree of heterogeneity. While the impact of small-scale heterogeneity can be effectively modelled by considering dispersivity as we have in this study, larger-scale heterogeneity would require a statistical approach involving multiple hydraulic conductivity fields (e.g. Mariethoz et al., 2009). Nonetheless, the results of this study provide useful quantitative guidelines for evaluating and estimating temporal and spatial aspects of contaminant plumes in layered sedimentary systems.

While the directions of the trends in the controls explored here can generally be deduced through logical reasoning informed by physics, the magnitude and interplay of these controls cannot. Cases wherein a confined or semi-confined aquifer contains a contaminant source zone (e.g., Jiménez-Martínez et al., 2011; Agah et al., 2013) are similar to the configuration of Scenarios A and C. If the hydraulic conductivity and thickness of the aquifer can be estimated, then the influence of diffusion constants and reaction rates on concentration and persistence can be evaluated (Figs. 3, 5, 6 and 9). This information can inform often costly decisions related to sampling efforts (e.g., which parameters field campaigns should seek to constrain) and remediation (e.g., whether or not to proceed with source zone treatment). For example, if the degradation rate can be increased by the addition of catalysts or reagents (e.g., Crane and Scott, 2012), then the potential improvement in plume persistence can be estimated. These considerations also hold for unconfined aquifers underlain by low-permeability layers (Scenario B). While the influences of the controls investigated here are less marked in this configuration, they nonetheless play important roles in determining the dynamics of contaminant plumes.

By using constructed parameters to reduce the dimensionality of the parameter space, general trends could be easily identified and specific regimes in which advection is the dominant control on plume persistence could be established. These parameters provide powerful predictive capacity for the evaluation of real systems. For example, in a confined aquifer, by estimating aquifer hydraulic conductivity, fluid diffusion constants, and reaction constants in the bounding low-permeability units, one can determine whether or not the system is in a low-persistence regime wherein the contaminant concentration will be rapidly attenuated. Furthermore, the fundamental relationship between equilibrium plume extent and the introduced parameter η should provide guidance for delimiting zones at risk of contamination. These types of calculations have strong potential for use in evaluations of plume persistence in contaminated sites.

This study provides novel quantitative information on the effects of advection, diffusion, sorption, degradation and layer thickness on the behaviour of contaminant plumes in sedimentary hydrogeological systems. It is our anticipation that this information on the relative influences of these controls in different situations serves to inform future evaluations of contaminated sites.

CRediT authorship contribution statement

Landon J.S. Halloran: Conceptualization, Methodology, Software, Validation, Formal analysis, Investigation, Resources, Data curation, Writing - original draft, Writing - review & editing, Visualization, Project administration. **Daniel Hunkeler:** Conceptualization, Investigation, Resources, Writing - review & editing, Supervision, Project administration, Funding acquisition.

Declaration of competing interest

The authors (Landon Halloran and Daniel Hunkeler) declare no competing interest.

Acknowledgements

The authors acknowledge the Swiss National Science Foundation (SNF/FNS) (grant number: 166233, https://p3.snf.ch/Project-166233) for its financial support. We thank Prof. Philip Brunner for his recommendations related to the Pi-Theorem. We also thank Editor Damia Barcelo and the anonymous reviewers for their helpful feedback.

Appendix A

The large amount of data generated and analysed in this study could not be included in its entirety. Readers are referred to the *python* code and associated data at https://github.com/lhalloran/ReactiveBackDiffusion2020 where they can produce modified versions of Figs. 3–10 by, for example, selecting any of the observation well locations (Fig. 1) and providing their own attenuation factor to extend the analysis presented in this manuscript.

References

Adamson, D.T., Mahendra, S., Walker, K.L., Rauch, S.R., Sengupta, S., Newell, C.J., 2014. A multisite survey to identify the scale of the 1,4-dioxane problem at contaminated groundwater sites. Environmental Science and Technology Letters 1 (5), 254–258. https://doi.org/10.1021/ez500092u.

Agah, A., Doulati Ardejani, F., Ghoreishi, H., 2013. Two-dimensional numerical finite volume modeling of processes controlling distribution and natural attenuation of BTX in the saturated zone of a simulated semi-confined aquifer. Arab. J. Geosci. 6 (6), 1933–1944. https://doi.org/10.1007/s12517-011-0467-4.

Allen-King, R.M., Groenevelt, H., Mackay, D.M., 1995. Analytical method for the sorption of hydrophobic organic pollutants in clay-rich materials. Environ. Sci. Technol. 29 (1), 148–153. https://doi.org/10.1021/es00001a019.

Badin, A., Buttet, G., Maillard, J., Holliger, C., Hunkeler, D., 2014. Multiple dual C-Cl isotope patterns associated with reductive dechlorination of tetrachloroethene. Environ. Sci. Technol. 48 (16), 9179–9186. https://doi.org/10.1021/es500822d.

Buckingham, E., 1914. On physically similar systems; illustrations of the use of dimensional equations. Phys. Rev. 4 (4), 345–376. https://doi.org/10.1103/PhysRev.4.345.

Cardenas, M.B., Wilson, J.L., 2007. Thermal regime of dune-covered sediments under gaining and losing water bodies. J. Geophys. Res. 112, G04013. https://doi.org/10.1029/2007JG000485.

Carey, G.R., Chapman, S.W., Parker, B.L., McGregor, R., 2015. Application of an adapted version of MT3DMS for modeling back-diffusion remediation timeframes. Remediat. J. 25 (4), 55–79. https://doi.org/10.1002/rem.21440.

Carlier, C., Wirth, S.B., Cochand, F., Hunkeler, D., Brunner, P., 2019. Exploring geological and topographical controls on low flows with hydrogeological models. Groundwater 57 (1), 48–62. https://doi.org/10.1111/gwat.12845.

Chapman, S.W., Parker, B.L., 2005. Plume persistence due to aquitard back diffusion following dense nonaqueous phase liquid source removal or isolation. Water Resour. Res. 41 (12), 1–16. https://doi.org/10.1029/2005WR004224.

Cirpka, O.A., Frind, E.O., Helmig, R., 1999. Numerical simulation of biodegradation controlled by transverse mixing. J. Contam. Hydrol. 40 (2), 159–182. https://doi.org/10.1016/S0169-7722(99)00044-3.

COMSOL AB, 2019. COMSOL Multiphysics User's Guide. 5.3 edition. COMSOL AB.

Crane, R., Scott, T., 2012. Nanoscale zero-valent iron: future prospects for an emerging water treatment technology. J. Hazard. Mater. 211–212, 112–125. https://doi.org/10.1016/j.jhazmat.2011.11.073.

Cretnik, S., Thoreson, K.A., Bernstein, A., Ebert, K., Buchner, D., Laskov, C., Haderlein, S., Shouakar-Stash, O., Kliegman, S., McNeill, K., Elsner, M., 2013. Reductive dechlorination of TCE by chemical model systems in comparison to dehalogenating bacteria: insights from dual element isotope analysis (13C/12C, 37Cl/35Cl). Environ. Sci. Technol. 47 (13), 6855–6863. https://doi.org/10.1021/es400107n.

Damgaard, I., Bjerg, P.L., Jacobsen, C.S., Tsitonaki, A., Kerrn-Jespersen, H., Broholm, M.M., 2013. Performance of full-scale enhanced reductive dechlorination in clay till. Groundwater Monitoring & Remediation 33 (1), 48–61. https://doi.org/10.1111/j.1745-6592.2012.01405.x.

Eberhardt, C., Grathwohl, P., 2002. Time scales of organic contaminant dissolution from complex source zones: coal tar pools vs. blobs. J. Contam. Hydrol. 59 (1–2), 45–66. https://doi.org/10.1016/S0169-7722(02)00075-X.

Falta, R.W., Suresh Rao, P., Basu, N., 2005. Assessing the impacts of partial mass depletion in DNAPL source zones. J. Contam. Hydrol. 78 (4), 259–280. https://doi.org/10.1016/j.jconhyd.2005.05.010.

Fick, A., 1855. Ueber diffusion. Annalen der Physik und Chemie 170 (1), 59–86. https://doi.org/10.1002/andp.18551700105.

Gelhar, L.W., Welty, C., Rehfeldt, K.R., 1992. A critical review of data on field-scale dispersion in aquifers. Water Resour. Res. 28 (7), 1955–1974. https://doi.org/10.1029/92WR00607.

Halloran, L.J., Brunner, P., Hunkeler, D., 2019. COMPEST, a PEST-COMSOL interface for inverse multiphysics modelling: development and application to isotopic fractionation of groundwater contaminants. Comput. Geosci. 126, 107–119. https://doi.org/10.1016/j.cageo.2019.02.001.

Hunkeler, D., Aravena, R., Berry-Spark, K., Cox, E., 2005. Assessment of degradation pathways in an aquifer with mixed chlorinated hydrocarbon contamination using stable isotope analysis. Environ. Sci. Technol. 39 (16), 5975–5981. https://doi.org/10.1021/es048464a.

Hunter, J.D., 2007. Matplotlib: a 2D graphics environment. Computing in Science & Engineering 9 (3), 90–95. https://doi.org/10.1109/MCSE.2007.55.

Huysmans, M., Dassargues, A., 2005. Review of the use of Péclet numbers to determine the relative importance of advection and diffusion in low permeability environments. Hydrogeol. J. 13 (5–6), 895–904. https://doi.org/10.1007/s10040-004-0387-4.

Jensen, K.H., Bitsch, K., Bjerg, P.L., 1993. Large-scale dispersion experiments in a sandy aquifer in Denmark: observed tracer movements and numerical analyses. Water Resour. Res. 29 (3), 673–696. https://doi.org/10.1029/92WR02468.

Jiménez-Martínez, J., Aravena, R., Candela, L., 2011. The role of leaky boreholes in the contamination of a regional confined aquifer. A case study: the campo de Cartagena region, Spain. Water Air Soil Pollut. 215 (1–4), 311–327. https://doi.org/10.1007/s11270-010-0480-3.

Kaplan, D.I., Denham, M.E., Zhang, S., Yeager, C., Xu, C., Schwehr, K.A., Li, H.P., Ho, Y.F., Wellman, D., Santschi, P.H., 2014. Radioiodine biogeochemistry and prevalence in groundwater. Crit. Rev. Environ. Sci. Technol. 44 (20), 2287–2335. https://doi.org/10.1080/10643389.2013.828273.

Lippmann-Pipke, J., Gerasch, R., Schikora, J., Kulenkampff, J., 2017. Benchmarking PET for geoscientific applications: 3D quantitative diffusion coefficient determination in clay rock. Comput. Geosci. 101, 21–27. https://doi.org/10.1016/j.cageo.2017.01.002.

Lu, X., Wilson, J.T., Kampbell, D.H., 2006. Relationship between Dehalococcoides DNA in ground water and rates of reductive dechlorination at field scale. Water Res. 40 (16), 3131–3140. https://doi.org/10.1016/j.watres.2006.05.030.

Majone, M., Verdini, R., Aulenta, F., Rossetti, S., Tandoi, V., Kalogerakis, N., Agathos, S., Puig, S., Zanaroli, G., Fava, F., 2015. In situ groundwater and sediment bioremediation: barriers and perspectives at European contaminated sites. New Biotechnol. 32 (1), 133–146. https://doi.org/10.1016/j.nbt.2014.02.011.

Mariethoz, G., Renard, P., Cornaton, F., Jaquet, O., 2009. Truncated Plurigaussian simulations to characterize aquifer heterogeneity. Ground Water 47 (1), 13–24. https://doi.org/10.1111/j.1745-6584.2008.00489.x.

Millington, R.J., Quirk, J.P., 1961. Permeability of porous solids. Trans. Faraday Soc. 57, 1200. https://doi.org/10.1039/tf9615701200.

Nardi, A., Idiart, A., Trinchero, P., De Vries, L.M., Molinero, J., 2014. Interface COMSOL-PHREEQC (iCP), an efficient numerical framework for the solution of coupled multiphysics and geochemistry. Comput. Geosci. 69, 10–21. https://doi.org/10.1016/j.cageo.2014.04.011.

Parker, B.L., Chapman, S.W., Guilbeault, M.A., 2008. Plume persistence caused by back diffusion from thin clay layers in a sand aquifer following TCE source-zone hydraulic isolation. J. Contam. Hydrol. 102 (1–2), 86–104. https://doi.org/10.1016/j.jconhyd.2008.07.003.

Rao, P.S.C., Jawitz, J.W., Enfield, C.G., Falta, R.W., Annable, M.D., Wood, A.L., 2002. Technology integration for contaminated site remediation: clean-up goals and performance criteria. IAHS-AISH Publication 275, 571–578.

Schaefer, C.E., Lippincott, D.R., Klammler, H., Hatfield, K., 2018. Evidence of rock matrix back-diffusion and abiotic dechlorination using a field testing approach. J. Contam. Hydrol. 209 (January), 33–41. https://doi.org/10.1016/j.jconhyd.2018.01.004.

Seyedabbasi, M.A., Newell, C.J., Adamson, D.T., Sale, T.C., 2012. Relative contribution of DNAPL dissolution and matrix diffusion to the long-term persistence of chlorinated solvent source zones. J. Contam. Hydrol. 134–135, 69–81. https://doi.org/10.1016/j.jconhyd.2012.03.010.

Smith, K.E., Thullner, M., Wick, L.Y., Harms, H., 2009. Sorption to humic acids enhances polycyclic aromatic hydrocarbon biodegradation. Environmental Science & Technology 43 (19), 7205–7211. https://doi.org/10.1021/es803661s.

Takeuchi, M., Kawabe, Y., Watanabe, E., Oiwa, T., Takahashi, M., Nanba, K., Kamagata, Y., Hanada, S., Ohko, Y., Komai, T., 2011. Comparative study of microbial dechlorination of chlorinated ethenes in an aquifer and a clayey aquitard. J. Contam. Hydrol. 124 (1–4), 14–24. https://doi.org/10.1016/j.jconhyd.2011.01.003.

Thouement, H.A.A., Kuder, T., Heimovaara, T.J., Breukelen, B.M.V., Van, B.M., 2019. Do CSIA data from aquifers inform on natural degradation of chlorinated ethenes in aquitards? J. Contam. Hydrol. 226 (May). https://doi.org/10.1016/j.jconhyd.2019.103520.

Vaschy, A., 1892. Sur les lois de similitude en physique. Annales Télégraphiques 19, 25–28.

Wanner, P., Parker, B.L., Chapman, S.W., Aravena, R., Hunkeler, D., 2016. Quantification of degradation of chlorinated hydrocarbons in saturated low permeability sediments using compound-specific isotope analysis. Environ. Sci. Technol. 50 (11), 5622–5630. https://doi.org/10.1021/acs.est.5b06330.

Wanner, P., Parker, B.L., Chapman, S.W., Aravena, R., Hunkeler, D., 2017. Does sorption influence isotope ratios of chlorinated hydrocarbons under field conditions? Appl. Geochem. 84, 348–359. https://doi.org/10.1016/j.apgeochem.2017.07.016.

Wanner, P., Parker, B.L., Chapman, S.W., Lima, G., Gilmore, A., Mack, E.E., Aravena, R., 2018a. Identification of degradation pathways of chlorohydrocarbons in saturated low-permeability sediments using compound-specific isotope analysis. Environ. Sci. Technol. 52 (13), 7296–7306. https://doi.org/10.1021/acs.est.8b01173.

Wanner, P., Parker, B.L., Hunkeler, D., 2018b. Assessing the effect of chlorinated hydrocarbon degradation in aquitards on plume persistence due to back-diffusion. Sci. Total Environ. 633, 1602–1612. https://doi.org/10.1016/j.scitotenv.2018.03.192.

Werth, C.J., Cirpka, O.A., Grathwohl, P., 2006. Enhanced mixing and reaction through flow focusing in heterogeneous porous media. Water Resour. Res. 42 (12), 1–10. https://doi.org/10.1029/2005WR004511.

Yang, M., Annable, M.D., Jawitz, J.W., 2015. Back diffusion from thin low permeability zones. Environmental Science & Technology 49 (1), 415–422. https://doi.org/10.1021/es5045634.

Yang, M., Annable, M.D., Jawitz, J.W., 2017. Field-scale forward and back diffusion through low-permeability zones. J. Contam. Hydrol. 202, 47–58. https://doi.org/10.1016/j.jconhyd.2017.05.001.

Yarin, L., 2012. The Pi-Theorem: Applications to Fluid Mechanics and Heat and Mass Transfer. Springer-Verlag.

Zakari, S., Liu, H., Tong, L., Wang, Y., Liu, J., 2016. Transport of bisphenol-A in sandy aquifer sediment: column experiment. Chemosphere 144, 1807–1814. https://doi.org/10.1016/j.chemosphere.2015.10.081.

Zimmermann, J., Halloran, L.J., Hunkeler, D., 2020. Tracking chlorinated contaminants in the subsurface using compound-specific chlorine isotope analysis: a review of principles, current challenges and applications. Chemosphere 244, 125476. https://doi.org/10.1016/j.chemosphere.2019.125476.